

# Parton distributions from deep-inelastic-scattering data

S. I. Alekhin

Institute for High Energy Physics, 142281 Protvino, Russia

## Abstract

We perform the analysis of existing light-targets deep-inelastic-scattering (DIS) data in the leading-order (LO), next-to-leading-order (NLO), and next-to-next-to-leading-order (NNLO) QCD approximations and extract PDFs simultaneously with the value of the strong coupling constant  $\alpha_s$  and the high-twist contribution to the structure functions. The main theoretical uncertainties and experimental uncertainties due to all sources of experimental errors in data are estimated, the latter generally dominate for the obtained PDFs. The uncertainty in Higgs boson production cross section due to errors in PDFs is  $\sim 2\%$  for the LHC and varies from 2% to 10% for the Fermilab collider under variation of the Higgs boson mass from 100 GeV to 300 GeV. For the  $W$ -boson production cross section the uncertainty is  $\sim 2\%$  for the both colliders. The value of  $\alpha_s^{\text{NNLO}}(M_Z) = 0.1143 \pm 0.0014(\text{exp.})$  is obtained, while the high-twist terms do not vanish up to the NNLO as required by comparison to data.

**PACS numbers:** 13.60.Hb, 06.20.Jr, 12.38.Bx

**Keywords:** deep inelastic scattering, parton distributions, strong coupling constant, high twists

# 1 Introduction

The deep-inelastic-scattering (DIS) data are used for extraction of the parton distribution functions (PDFs) in nucleon starting from the advent of the Bjorken scaling phenomena (for the most recent studies see Refs. [1, 2, 3]). However since new DIS data appear permanently and the theoretical basis for their analysis is being developed alongside, those analysis should be updated in order to improve the experimental and theoretical errors on the extracted PDFs. In this paper we give such update of the next-to-leading-order (NLO) QCD analysis of Ref. [3] aimed to extract PDFs, the high-twist (HT) contribution to the structure functions  $F_{2,L}$ , and the value of strong coupling constant  $\alpha_s$  from the existing data on DIS of charged leptons off the proton and deuterium targets. One of the improvements of our analysis is replacement of data by the H1 [4] and the ZEUS [5] collaborations by their more recent data [6, 7] obtained in the 1996-97 run of the HERA collider, when these experiments accumulated about 5 times more events than before. Another improvement is account of the NNLO QCD corrections, which have been known with a good precision after calculation of the Mellin moments of the NNLO splitting functions up to 14-th [8]. This new input significantly decreases the uncertainty of PDFs due to the higher-orders (HO) QCD corrections [9, 10] and together with more precise data allows to produce the NLO and NNLO PDFs sets with reduced total uncertainty.

The particular features of the analysis [3] as compared to the global fits of Refs.[11, 12] are:

- data on the differential cross sections are used that allows to use experimental constraints on the structure function  $F_L$ ;
- corrections for the effects of target mass (TM) and for the nuclear effects in deuteron are applied to the data, the both were calculated in the fits iteratively using the current PDFs;
- comprehensive account of the experimental errors and their correlations is performed;
- impact of main sources of the theoretical errors is analyzed.

All these features are also kept in the present analysis.

Table 1: The numbers of data points (NDP) for separate experiments and the corresponding renormalization shifts  $\xi$  obtained in different fits.

Experiment	NDP	proton			NDP	deuterium		
		$\xi[\%]$				$\xi[\%]$		
		LO	NLO	NNLO		LO	NLO	NNLO
SLAC-E-49A	58	$2.9 \pm 1.4$	$1.6 \pm 1.4$	$1.1 \pm 1.4$	58	$0.0 \pm 1.3$	$-1.3 \pm 1.3$	$-1.7 \pm 1.3$
SLAC-E-49B	144	$3.2 \pm 1.4$	$1.8 \pm 1.4$	$1.2 \pm 1.4$	135	$0.5 \pm 1.4$	$-0.8 \pm 1.4$	$-1.3 \pm 1.4$
SLAC-E-87	90	$2.9 \pm 1.4$	$1.8 \pm 1.4$	$1.2 \pm 1.4$	90	$0.7 \pm 1.3$	$-0.5 \pm 1.3$	$-0.9 \pm 1.3$
SLAC-E-89A	66	$5.6 \pm 1.9$	$4.0 \pm 1.9$	$3.1 \pm 1.9$	59	$2.3 \pm 2.0$	$0.5 \pm 2.0$	$-0.3 \pm 2.0$
SLAC-E-89B	79	$2.6 \pm 1.3$	$1.2 \pm 1.4$	$0.7 \pm 1.4$	62	$-0.2 \pm 1.3$	$-1.4 \pm 1.3$	$-1.9 \pm 1.4$
SLAC-E-139					16	$1.6 \pm 1.3$	$0.2 \pm 1.3$	$-0.2 \pm 1.3$
SLAC-E-140					26			
BCDMS	351				254			
NMC(90 GeV)	46	$-1.5 \pm 1.6$	$-1.4 \pm 1.5$	$-1.3 \pm 1.6$	46	$-2.6 \pm 1.5$	$-3.0 \pm 1.5$	$-2.9 \pm 1.5$
NMC(120 GeV)	59	$-0.2 \pm 1.5$	$0.2 \pm 1.5$	$0.4 \pm 1.5$	59	$-1.3 \pm 1.5$	$-1.6 \pm 1.4$	$-1.5 \pm 1.5$
NMC(200 GeV)	66	$2.1 \pm 1.5$	$1.9 \pm 1.4$	$2.0 \pm 1.4$	66	$0.0 \pm 1.4$	$-0.3 \pm 1.4$	$-0.3 \pm 1.4$
NMC(280 GeV)	74	$1.3 \pm 1.4$	$0.9 \pm 1.4$	$0.8 \pm 1.4$	74	$-1.1 \pm 1.4$	$-1.4 \pm 1.4$	$-1.4 \pm 1.4$
H1	135							
ZEUS	161							

## 2 Theoretical and experimental input of the fit

The model for data description is based on perturbative QCD with phenomenological parameterization of the LT and HT contributions to the structure functions  $F_{2,L}$ . The analysis was performed in the  $\overline{\text{MS}}$  scheme with the number of flavors fixed at 3. The LT PDFs are parameterized at  $Q_0^2 = 9 \text{ GeV}^2$  in the following form:

$$xu_V(x, Q_0) = \frac{2}{N_u^V} x^{a_u} (1-x)^{b_u} (1 + \gamma_2^u x), \quad (1)$$

$$xu_S(x, Q_0) = \frac{A_S}{N_S} \eta_u x^{a_s} (1-x)^{b_{su}}, \quad (2)$$

$$xd_V(x, Q_0) = \frac{1}{N_d^V} x^{a_d} (1-x)^{b_d}, \quad (3)$$

$$xd_S(x, Q_0) = \frac{A_S}{N_S} x^{a_s} (1-x)^{b_{sd}}, \quad (4)$$

$$xs_S(x, Q_0) = \frac{A_S}{N_S} \eta_s x^{a_s} (1-x)^{(b_{su}+b_{sd})/2}, \quad (5)$$

$$xG(x, Q_0) = A_G x^{a_G} (1-x)^{b_G} (1 + \gamma_1^G \sqrt{x} + \gamma_2^G x), \quad (6)$$

where  $u, d, s, G$  are the up, down, strange quarks, and gluons distributions respectively; indices  $V$  and  $S$  correspond to the valence and sea quarks. The parameters  $N_u^V, N_d^V$  and  $A_G$  were calculated from the other parameters using conservation of the partons momentum and the fermion number. The normalization parameter  $N^S$  is selected in such way that  $A_S$  gives the total momentum carried by the sea quarks. The parameter  $\eta_s$  was fixed at 0.42, in agreement with the results of NuTeV collaboration [13]. The rest of parameters coming to Eqns.(1–6) were fitted to the data, we convinced that no extra parameters are needed to improve the data description. The HT contributions to the fitted structure functions  $F_{2,L}$  were parameterized in additive form

$$F_{2,L} = F_{2,L}^{\text{LT,TMC}} + \frac{H_{2,L}(x)}{Q^2},$$

Table 2: The values of  $\chi^2/\text{NDP}$  for different fits and of the averages of residuals  $R$  for the NLO fit together with their standard deviations  $\Delta R$  for separate data sets used in the analysis.

Experiment	NDP	$\chi^2/\text{NDP}$			$R(\Delta R)$
		LO	NLO	NNLO	
SLAC-E-49A	115	0.54	0.52	0.52	$-0.04(0.23)$
SLAC-E-49B	279	1.27	1.20	1.21	$0.23(0.29)$
SLAC-E-87	180	0.96	0.92	0.91	$0.01(0.37)$
SLAC-E-89A	125	1.35	1.33	1.36	$-0.18(0.45)$
SLAC-E-89B	141	0.94	0.82	0.81	$0.47(0.49)$
SLAC-E-139	16	0.81	0.58	0.62	$-0.07(0.43)$
SLAC-E-140	26	1.31	0.94	0.90	$0.17(0.86)$
BCDMS	605	1.15	1.13	1.12	$-0.06(0.68)$
NMC	490	1.35	1.24	1.24	$-0.06(0.39)$
H1(96-97)	135	1.39	0.97	1.09	$0.42(0.55)$
ZEUS(96-97)	161	1.54	1.32	1.28	$-0.55(0.64)$
TOTAL	2274	1.20	1.11	1.11	$0.01(0.22)$

where  $F_{2,L}^{\text{LT,TMC}}$  are the LT terms with account of the TM correction<sup>1</sup> and functions  $H(x)$  are parameterized in the piece-linear form and fitted to the data.

The code used to evolve these distributions was used earlier in the analysis of Ref. [10]. This code was checked against Les Houches benchmark of Ref.[14] and demonstrated accuracy much better than experimental precision of the analyzed data. A brief description of the data sets used in the analysis is given in Table 1. We cut data with  $Q^2 < 2.5 \text{ GeV}^2$ ,  $Q^2 > 300 \text{ GeV}^2$ , and  $x > 0.75$  in order to minimize effects of the higher-order QCD corrections, electroweak interference, and uncertainties in the TM and deuteron corrections correspondingly. All experimental uncertainties in data released by authors were accounted for in the analysis, including statistical errors and correlated systematical errors (in particular the general normalization errors).

The total normalization of the NMC and most of the SLAC data subsets

---

<sup>1</sup>See Ref. [3] for detailed formula.

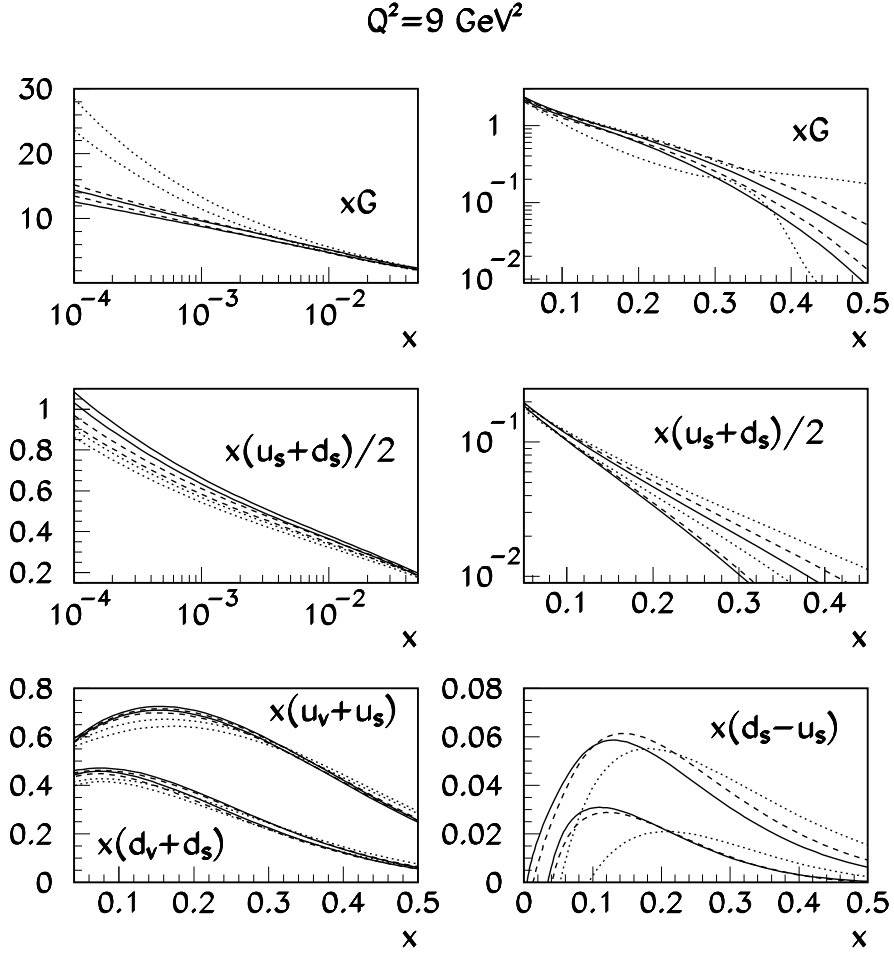


Figure 1: The experimental (statistical and systematical) errors bands for the PDFs obtain in the LO (dots), NLO (dashes), and NNLO (full) fits.

used in our analysis were not determined in the experiments, instead they were fitted by authors to the results of other experiments. Since now we have more DIS data than it was used in those fits, we perform independent renormalization of the NMC and SLAC data subsets that allows for more precise determination of the corresponding normalization factors. Following the approaches adopted by those experimental groups we introduce an additional normalization parameter for each beam energy and target in the NMC data set and for each experiment and target in the SLAC data sets. The data from SLAC-E-140 experiment, which was performed with particular attention paid to the accurate determination of the absolute normalization, were not renormalized – we accounted for its general normalization error given by the authors in the same way as the other correlated systematic errors. The same approach was used for treatment of the general normalization error in the BCDMS, H1, and ZEUS data. The normalization factors for the SLAC and NMC data are given in Table 1 for the fits performed in the LO, NLO, and NNLO approximations. In the LO fit the shifts for the SLAC deuterium sets deviate off zero by about two standard deviations, while for the NNLO fit they vanish, i.e. account of the higher-order corrections decreases tension between the different data sets (evidently, this effect is less pronounced for the NMC data than for the SLAC one since the later correspond to the lower values of  $Q$ , where these corrections are more important). In average, renormalization of the SLAC data sets in the NLO fit is  $\sim +2\%$  for the proton and  $\sim -0.5\%$  for the deuterium targets. For the NMC data the corresponding values also are different and, besides, vary with the beam energy that justifies application of the flexible renormalization scheme for this experiment. Note that in particular due to this flexible renormalization we obtain satisfactory description of the NMC data in the NLO:  $\chi^2/\text{NDP}=1.24$  in contrast with value 1.5 obtained in the fit of Ref. [11]. The values of  $\chi^2/\text{NDP}$  obtained in different orders of QCD are given in Table 2. One can see that quality of the fit is approximately the same for the NLO and NNLO fits and much worse for the LO fit.

### 3 PDFs and their experimental errors

The PDFs obtained from the fits in different pQCD orders with their total experimental uncertainties are given in Fig.1, the PDFs parameters are given in Table 3. One can see that the shift between the NLO and NNLO

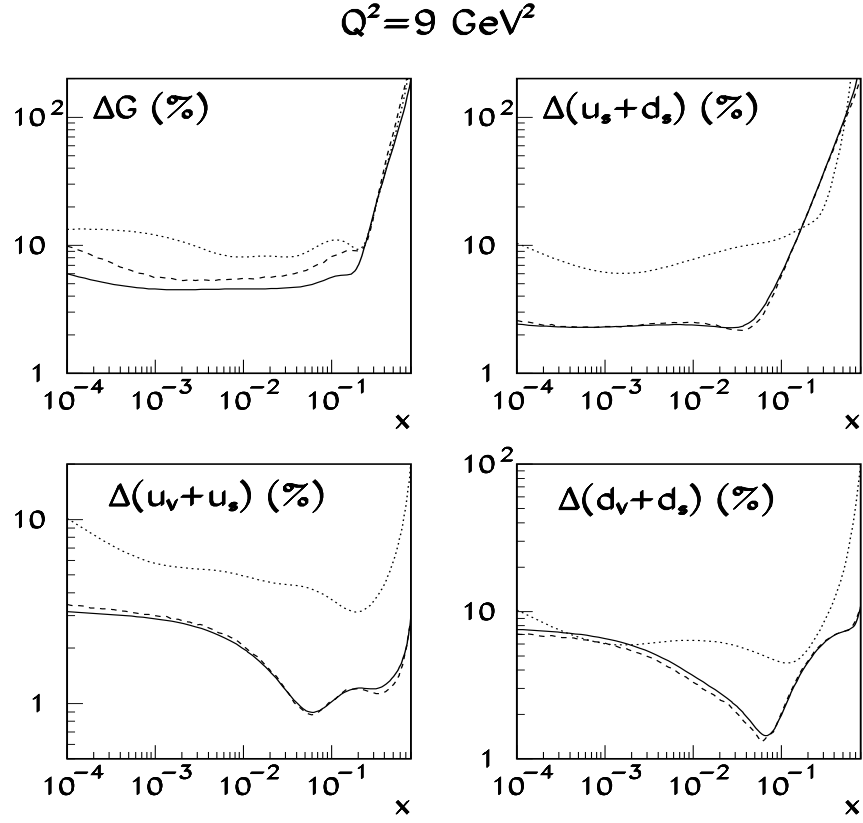


Figure 2: Impact of changes in the data set on the NLO PDFs and their errors. Full lines: relative experimental errors in our PDFs; dashes: the same for the PDFs of Ref. [3]; dots: the same for the CTEQ6 PDFs.



PDFs is generally within their experimental errors excluding the sea quarks distribution at small  $x$ . The LO gluon distribution at small  $x$  and valence quarks distributions at moderate  $x$  are very different from the corresponding NLO and NNLO PDFs. This difference cannot be completely ascribed to the re-definition of PDFs in different orders since data are poorly described by pQCD in the LO. Fitted LO PDFs are evidently distorted due to inaccount of the HO corrections and this distortion should be taken into account in calculation of other hard processes in the LO approximation. The PDFs errors consecutively fall from LO to NNLO due to additional terms of the perturbative expansions put additional constraints on the fitted values. This effect is most pronounced for the gluon distribution at large  $x$ . The comparison with experimental uncertainties in the NLO PDFs obtained from our earlier analysis of Ref. [3] is given in Fig.2. The main improvement is in precision of the gluon distribution at small  $x$  due to more precise HERA data have been used. The total experimental errors can be conventionally split into 3 components: the uncorrelated, general normalization, and correlated errors (excluding normalization ones). The normalization errors can also be considered as correlated ones, but we separate them for the purpose of comparison since very often the normalization errors are accounted for in a peculiar way or not accounted for at all. In our analysis the normalization errors for BCDMS, H1, and ZEUS data sets are included in the general covariance matrix, while for SLAC and NMC data sets they appear through the error matrix of the fitted parameters. Ratios of the correlated errors to the uncorrelated ones and of the normalization errors to the correlated ones for different PDFs are given in Fig.3. One can see that for most of PDFs the correlated errors are more important at small  $x$ . The normalization errors are largest at large  $x$ ; in this region they give main contribution to the total experimental uncertainties in PDFs.

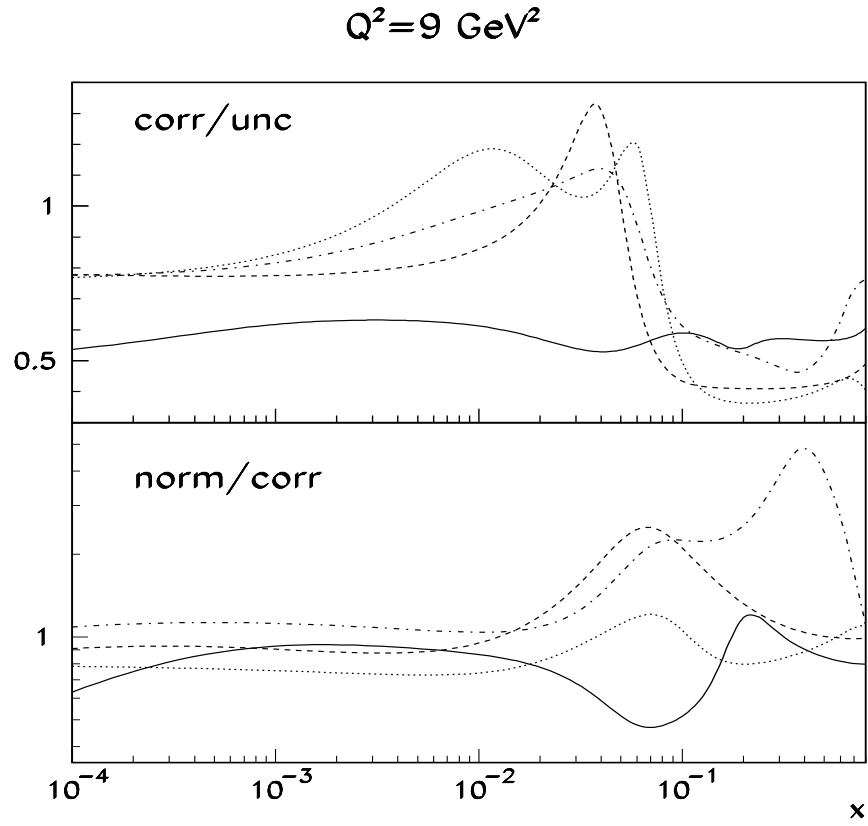


Figure 3: Ratios of the correlated systematic errors to the uncorrelated ones (upper panel) and of the normalization errors to the correlated ones (lower panel) for different PDFs (full curves: gluons; dashes: sea quarks; dots:  $d$ -quarks, dashed-dots:  $u$ -quarks).

Table 3: The values of the fitted parameters of the PDFs.

		LO	NLO	NNLO	
				(A+B)/2	B
Valence					
	$a_u$	$0.551 \pm 0.085$	$0.700 \pm 0.030$	$0.725 \pm 0.027$	$0.725 \pm 0.026$
	$b_u$	$3.672 \pm 0.042$	$3.920 \pm 0.050$	$4.024 \pm 0.050$	$4.011 \pm 0.050$
	$\gamma_2^u$	$3.0 \pm 1.7$	$1.14 \pm 0.39$	$1.05 \pm 0.35$	$1.01 \pm 0.34$
	$a_d$	$0.639 \pm 0.047$	$0.722 \pm 0.082$	$0.772 \pm 0.074$	$0.818 \pm 0.062$
	$b_d$	$4.48 \pm 0.23$	$4.94 \pm 0.12$	$5.14 \pm 0.15$	$5.22 \pm 0.18$
Glue					
	$a_G$	$-0.302 \pm 0.021$	$-0.146 \pm 0.018$	$-0.128 \pm 0.021$	$-0.096 \pm 0.020$
	$b_G$	$5.3 \pm 5.1$	$8.2 \pm 1.3$	$9.4 \pm 1.1$	$9.8 \pm 1.0$
	$\gamma_1^G$	$-1.94 \pm 0.83$	$-3.76 \pm 0.45$	$-3.84 \pm 0.52$	$-4.18 \pm 0.45$
	$\gamma_2^G$	$2.8 \pm 5.3$	$7.7 \pm 1.7$	$8.6 \pm 1.7$	$9.2 \pm 1.5$
Sea					
	$A_S$	$0.161 \pm 0.013$	$0.160 \pm 0.011$	$0.1591 \pm 0.0090$	$0.1545 \pm 0.0071$
	$a_{sd}$	$-0.1980 \pm 0.0057$	$-0.1968 \pm 0.0048$	$-0.2092 \pm 0.0044$	$-0.2086 \pm 0.0043$
	$b_{sd}$	$3.8 \pm 1.1$	$5.1 \pm 1.4$	$5.6 \pm 1.3$	$6.5 \pm 1.1$
	$\eta_u$	$1.46 \pm 0.15$	$1.16 \pm 0.12$	$1.12 \pm 0.11$	$1.036 \pm 0.099$
	$b_{su}$	$9.2 \pm 1.8$	$10.16 \pm 0.93$	$10.49 \pm 0.90$	$10.43 \pm 0.89$

Impact of each data set on the precision of our PDFs is demonstrated in Fig.4. The HERA data are crucial for determination of the gluon and quarks distributions at small  $x$ ; the BCDMS data constraint the quark distributions at large  $x$ ; the NMC data are essential for determination of the anti-quarks and  $d$ -quark distributions at large  $x$ ; and the SLAC data improve precision of the  $d$ -quark and gluon distributions at large  $x$ . In summary none of the subsets can be dropped out without deterioration of the PDFs precision. We also checked how sensitive are the errors in PDFs to the inclusion in fit the ZEUS data of Ref. [7] with  $Q^2 > 250 \text{ GeV}^2$ , the H1 data of Ref. [16] with  $Q^2 > 150 \text{ GeV}^2$ , and the FNAL-E-665 data of Ref. [17]. If one applies to these data our regular kinematical cuts  $Q^2 > 2.5 \text{ GeV}^2$  and  $x < 0.75$ , the relative suppression of the PDFs errors after each of these data sets has been included does not exceed 0.9 and therefore they are useless for the PDFs determination.

The novel HERA data used in our fit is confronted with the fitted curves in Figs.5,6. For comparison we show in the same figures the calculations based on our earlier PDFs of Ref.[3]. The experimental error bands for both sets of PDFs overlap that proves stability of the analysis. If the fit is unbiased, the fitted curve and data should coincide modulo statistical fluctuations. These fluctuations are quantified by the average of residuals  $R = \langle (f - y)/e \rangle$ , where  $f$  is the fitted function,  $y$  is measurement, and  $e$  is the total experimental error in data. The standard deviation of this average  $\Delta R$  is  $\sim 1/\sqrt{NDP}$  for data set with uncorrelated points. If data are correlated, coherent shift of the fitted curve within the value of common systematic error in data is allowed and value of  $\Delta R$  gets larger, up to 1 for the case of strong correlations. Therefore the value of  $\Delta R$  can be used as a crude indicator of significance of correlations in data set. In our analysis  $\Delta R$  is largest for the BCDMS and SLAC-E-140 data (see Table 2). Since magnitudes of  $R$  are well within  $\Delta R$  both for all subsets and for the total set we conclude that our fit is unbiased. Despite the systematic errors are not necessarily Gaussian distributed the value of  $\chi/NDP = 1.1$  obtained in our fit proves that this is good approximation in our case. Distribution of the diagonalized residuals (DRs), which are the components of the vector of residuals  $(f - y)/e$  multiplied by the square root of the inverse covariance matrix is plotted in Fig.7. If the errors obey the Gaussian distribution the distribution of DRs have to be normal [15] and as one can see in Fig.7 this is the case for our fit. Therefore all errors are Gaussian in good approximation

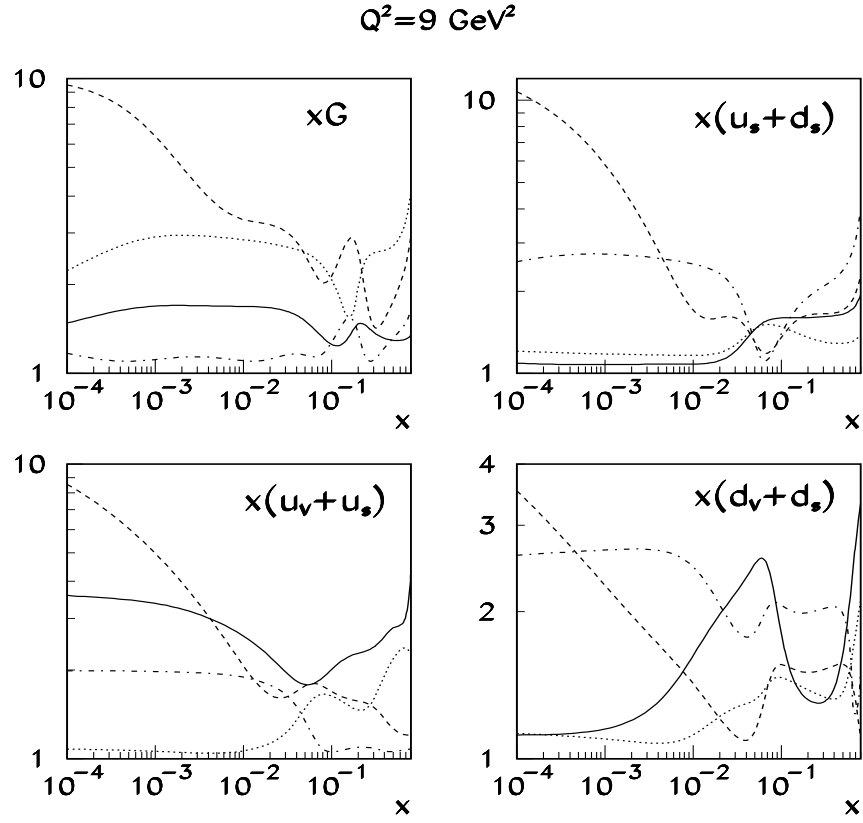


Figure 4: Relative increase of the experimental errors in our NLO PDFs due to rejection of different data sets from the fit (full curves: BCDMS data are rejected; dashes: HERA ones; dots: SLAC ones; dashed-dots: NMC ones).

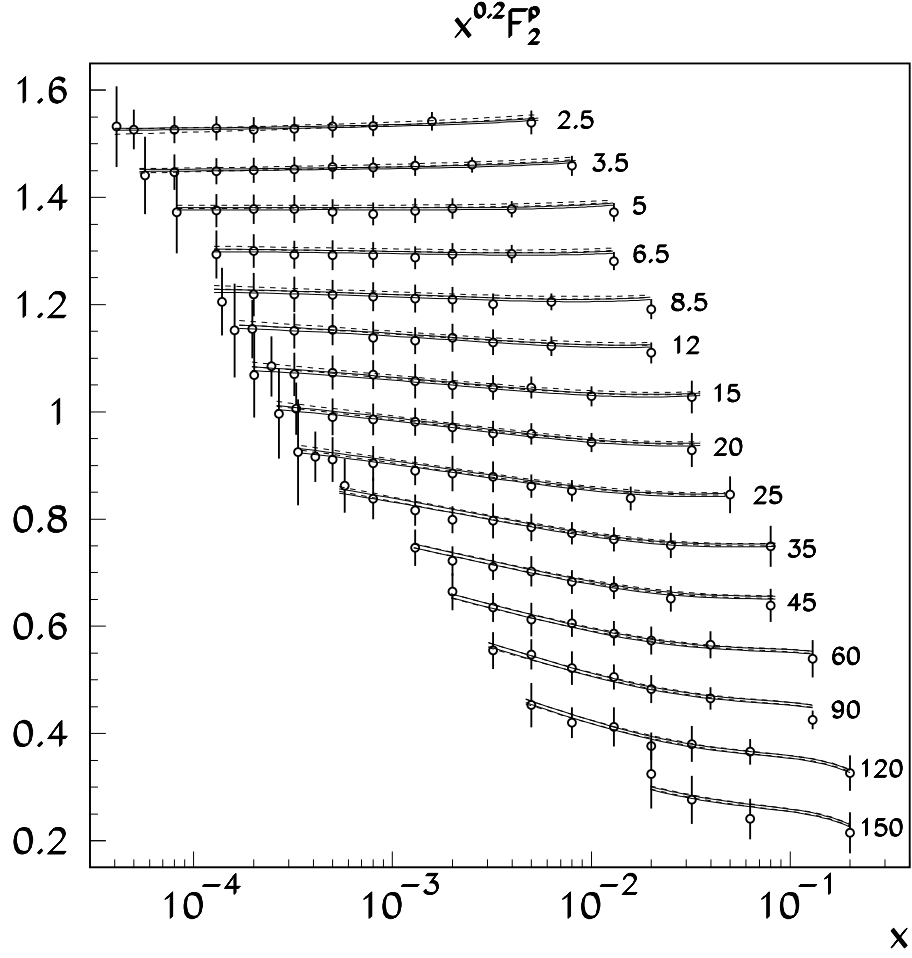


Figure 5: The experimental error bands for  $F_2^p$  calculated using our NLO PDFs (full curves) compared to the H1 data used in the fit. Figures at the curves are values of  $Q^2$  in units of  $\text{GeV}^2$ . For better view the factor of  $x^{0.2}$  and vertical shifts are applied to the data points and curves. The same bands calculated using the A99 PDFs are also given for comparison (dashed curves).

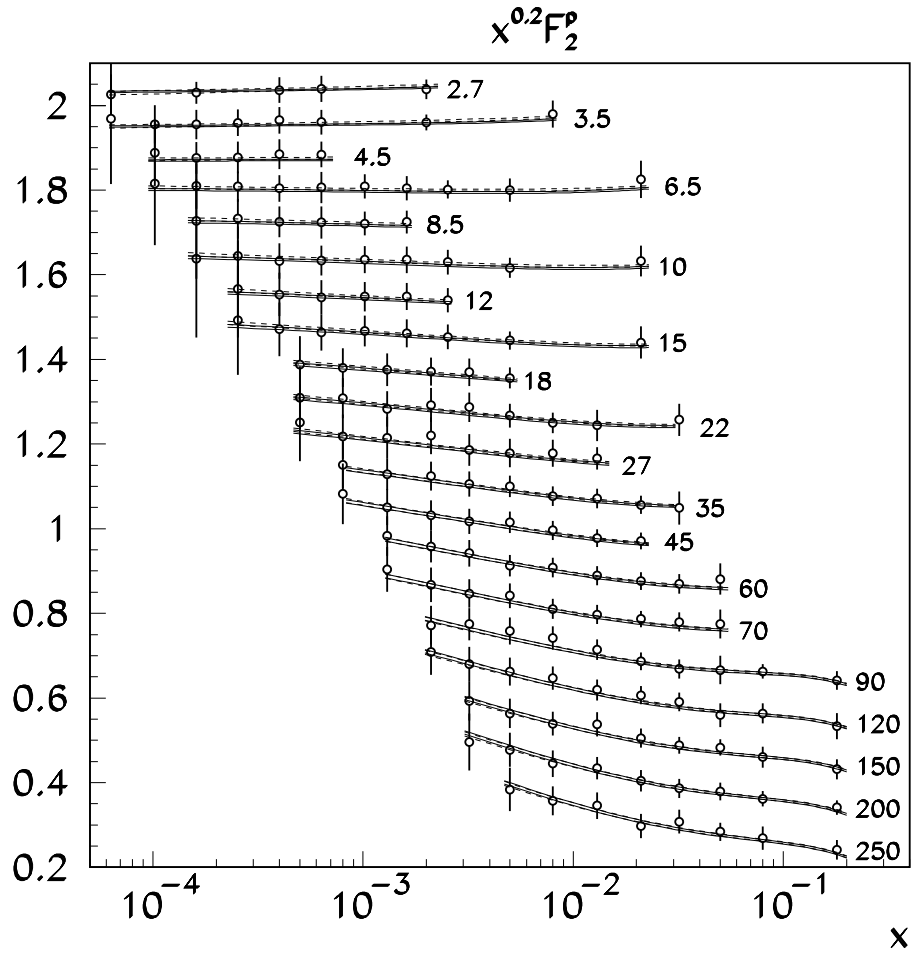


Figure 6: The same as Fig.5 for the ZEUS data used in the fit.

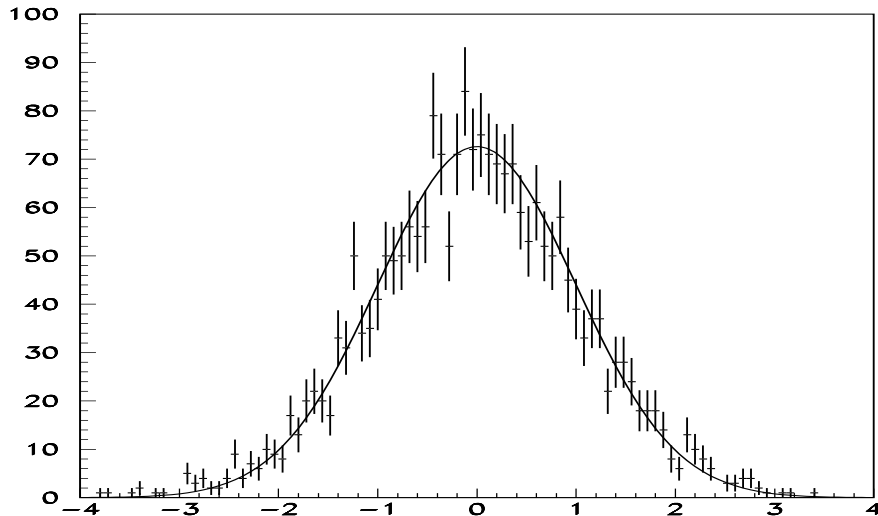


Figure 7: Distribution of the diagonalized residuals in our NLO fit. The curve superimposed gives normal distribution.

and consequently the errors in fitted parameters are Gaussian too<sup>2</sup>.

## 4 The PDFs theoretical uncertainties

With experimental errors in PDFs permanently reduced due to more relevant data appear the theoretical errors become more dominating contribution to the total PDFs uncertainty. In study of the importance of theoretical uncertainties the experimental errors serve as a natural scale. The variations below this scale can be neglected and, moreover, they just can occur due to statistical fluctuations in data. For this reason we analyzed only the theoretical errors, which give effect larger or comparable to the experimental ones.

---

<sup>2</sup>The width of the DRs distribution is 1.05 that is marginally larger than the width of the normal one; for this reason rescaling of the errors in spirit of the PDG's procedure would lead to negligible effect.



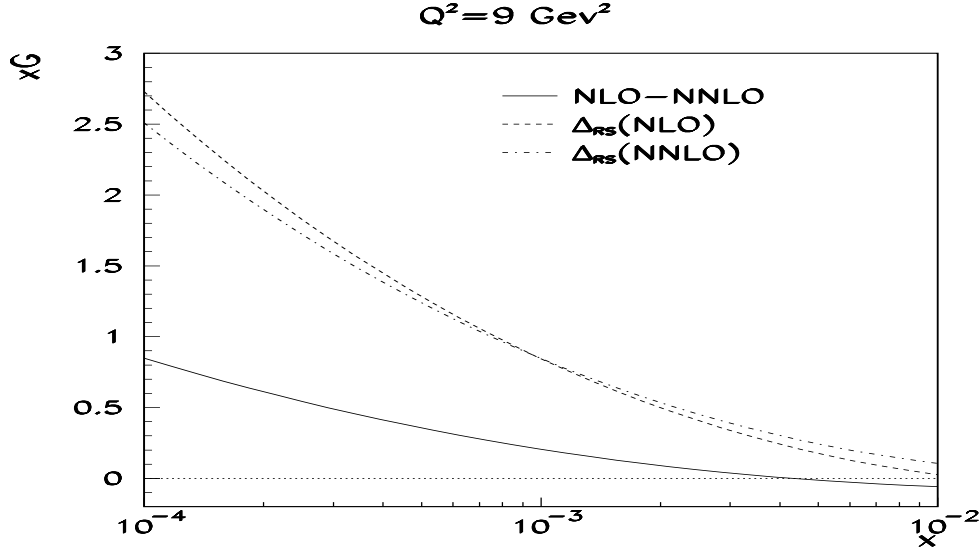


Figure 8: Perturbative stability of the gluon distribution at small  $x$ . The corresponding RS error  $\Delta_{RS}$  in the NLO and NNLO is given for comparison.

#### 4.1 Uncertainty due to higher order QCD corrections

The uncertainty in PDFs due to the HO QCD corrections is not an uncertainty in full sense because the PDFs differ from order to order just by definition. Nevertheless the variation of PDFs with the pQCD order is of practical importance for estimation of the HO QCD uncertainties in the hard cross sections, which are calculated using the PDFs, despite the variation of the cross section value due to the HO corrections to PDFs can be in some cases partially compensated by the HO corrections to the corresponding coefficient functions. A common approach used for estimation of the HO errors in the analysis of DIS data is to vary the QCD renormalization scale (RS) and factorization scale (FS) from  $Q^2$  to  $4Q^2$ . Evidently, since the range of this variation is arbitrary and no  $x$ -dependence of the scale factors is assumed, this approach gives only semi-qualitative estimate on the HO uncertainty. Having the PDFs at different pQCD orders we can verify this approach comparing the real variation of PDFs from order to order with the HO errors estimated using the variation of the pQCD scales. Example of such comparison is given in Fig.8. One can see that the real change of the

gluon distribution from the NLO to the NNLO is much smaller than the RS error at small  $x$ . With the FS errors taken into account the difference would get even larger. Adjustment of the range of the scale variation would also not help since the signs of the NLO-NNLO difference and the RS error are opposite at  $x \sim 0.01$ . Note that the RS error in gluon distribution almost does not decrease from the NLO to the NNLO. This means that if the perturbative expansion does converge the discrepancy between the NNLO RS error and the change of gluon distribution from the NNLO to the NNNLO is even larger. For this reason we recommend to use the difference between NLO and NNLO PDFs as estimate of the HO uncertainty motivated by the properties of the asymptotic expansions. The NNLO PDFs have an additional source of errors due to possible variation of the NNLO kernel. The magnitude of these errors is largest at small  $x$ , but even in this region they are smaller than the experimental errors (see Fig.9).

## 4.2 Uncertainties due to the heavy quarks contribution

### 4.2.1 Variation of the factorization scheme

In our analysis contribution of the  $c$ - and  $b$ -quarks was calculated in the fixed-flavor-number (FFN) scheme using the photon-gluon fusion mechanism [18] with account of the NLO QCD correction [19]. Since the heavy-quark contribution rises with  $Q$  rapidly the FFN scheme without resummation of large logs is irrelevant at small  $x$  and  $Q$  much larger than the quark mass [20]. In order to overcome this difficulty the variable-flavor-number (VFN) scheme was proposed [21]. In the VFN scheme the heavy quarks are considered as massless and are included in the QCD evolution at  $Q = m_{c,b,t}$ , where  $m_{c,b,t}$  are the masses of  $c$ -,  $b$ -, and  $t$ -quark correspondingly. The VFN scheme does include resummation of large logs, but at the same time evidently overestimates the heavy-quarks distributions at  $Q$  close to the thresholds. Nevertheless this scheme is widely used in practice due to it allows for to greatly simplify the calculation of processes with the heavy quarks involved. The FFN scheme is appropriate in our case since the heavy-quarks contribution is concentrated at small  $x$ , while the small  $x$  data used in our analysis correspond to the values of  $Q$ , which are not very far from the threshold of heavy quarks production. Nevertheless in order to lighten implementation of our PDFs in different calculations we generated the VFN PDFs using our FFN

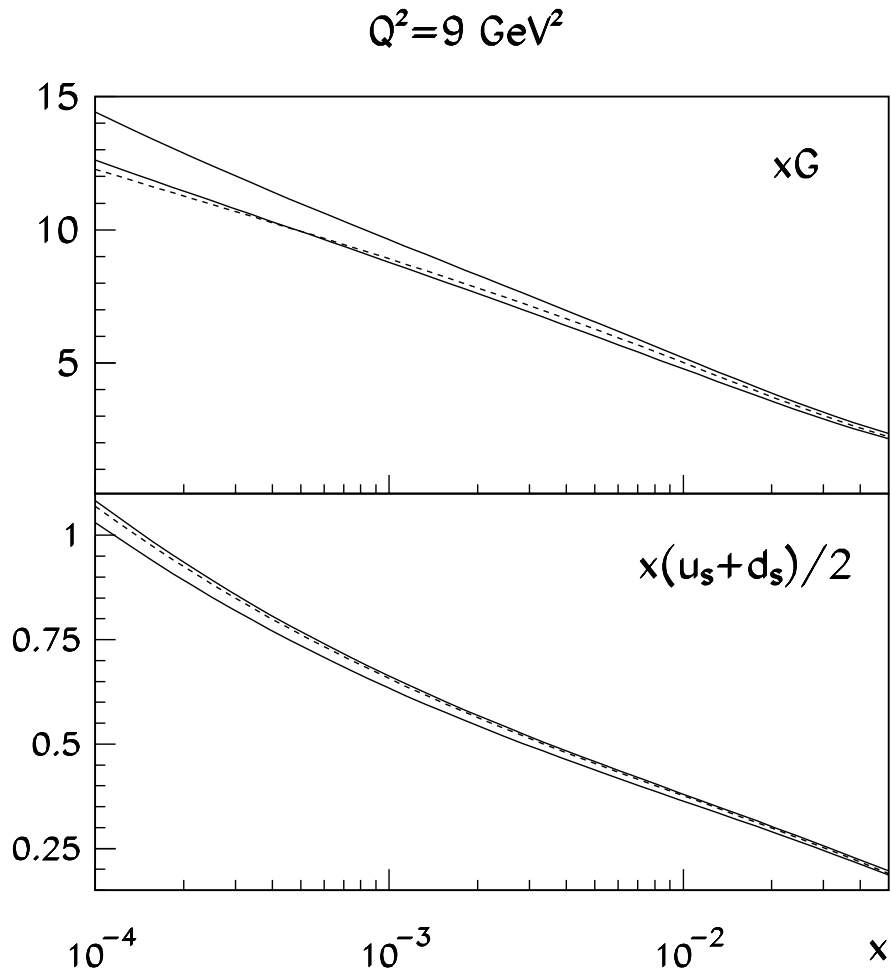


Figure 9: The NNLO PDFs obtained with the different choices of the NNLO kernel (full lines:  $1\sigma$  experimental bands for the nominal fit; dashes: fit with the NNLO kernel modified within the allowed uncertainty given in Ref.[9]).

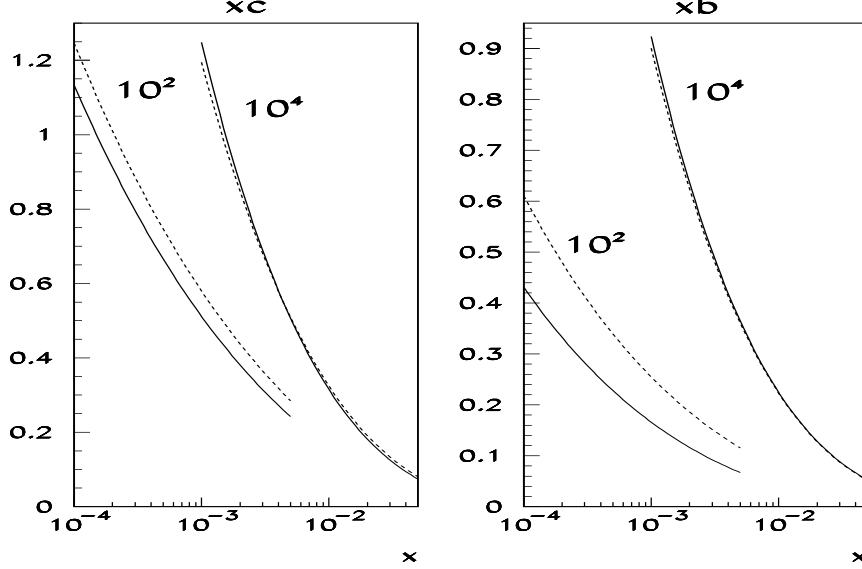


Figure 10: The  $c$ - and  $b$ -quarks distributions in the VFN scheme (dashed curves) compared to the corresponding FFN contributions to the structure function  $F_2$  weighted with the quarks charges (full curves). The figures at the curves give the values of  $Q^2$  in  $\text{GeV}^2$ ; the range of  $x$  for a given  $Q^2$  is typical for the processes studied at the Fermilab and LHC colliders.

PDFs as input. For this purpose we evolved our PDFs from our boundary value of  $Q_0^2 = 9 \text{ GeV}^2$  to  $Q = m_c$  in the FFN scheme and used the obtained PDFs as the boundary condition for the VFN evolution. The obtained VFN distributions of  $c$ - and  $b$ -quarks in the NLO are given in Fig.10 in comparison with the corresponding contributions to the structure function  $F_2$  calculated in the FFN scheme and weighted for the quarks charges. At large  $Q$  the FFN scheme gives results similar to the VFN ones at the values of  $x$  feasible by future hadron colliders. At low  $Q$  the VFN scheme gives sizeable overestimation of the heavy-quark distributions, especially for the  $b$ -quarks. For this reason the certain caution is necessary in use of the VFN PDFs at small  $Q$  (see also Ref. [22] in this connection).

### 4.2.2 Uncertainty due the error in heavy quarks masses

This uncertainty is estimated as the variation of PDFs under the change of  $m_c$  from 1.5 GeV to 1.75 GeV, i.e. within the error in its value estimated from other measurements. The magnitude of corresponding uncertainties in PDFs decreases from the LO to the NNLO since the HO PDFs are smoother at small  $x$  and variation of the photon-gluon fusion cross section gets less sensitive to the shift of the kinematical variables. The ratio of its magnitude to the PDFs experimental errors in the NLO is given in Fig.11. The ratio is generally less than 1.5 being most important for the sea quarks distribution at small  $x$ . The similar ratio for uncertainty due to variation of the  $b$ -quark mass is negligible for all PDFs.

### 4.3 Uncertainty due to variation of the strange sea parameterization

The  $s$ -quark distribution equally contributes to all structure functions of the charged leptons DIS and cannot be determined from these data due to lack of constraints. Most precise information about this distribution comes from the neutrino nucleon DIS data. Its shape was determined by the NuTeV collaboration to be comparable to the average of the  $u$ - and  $d$ -quarks distributions and the total suppression factor of the  $s$ -quark distribution  $\eta_s$  was found to be  $0.42 \pm 0.07(\text{stat.}) \pm 0.06(\text{syst.})$  [13]. We estimate the uncertainty in PDFs due to error in the  $s$ -quark distribution as change of the PDFs under variation of  $\eta_s$  from 0.42 to 0.52. This uncertainty marginally changes from the LO to the NNLO and does not exceed the PDFs experimental errors (see Fig.11).

### 4.4 Other theoretical errors

The list of possible theoretical errors in PDFs is rather conventional. For example the errors due to HT contribution can be estimated as shift of the fitted PDFs under addition to the power-like terms with the  $x$ -shape motivated by a certain model considerations to the fitted function. Alternatively, it can be accounted for by fitting possible HT contribution in the model-independent form; in this case the error due to the HT is combined with the total experimental error in PDFs. Since the later approach is less subjective we use it in our analysis. Similarly, we do not treat the error due to the

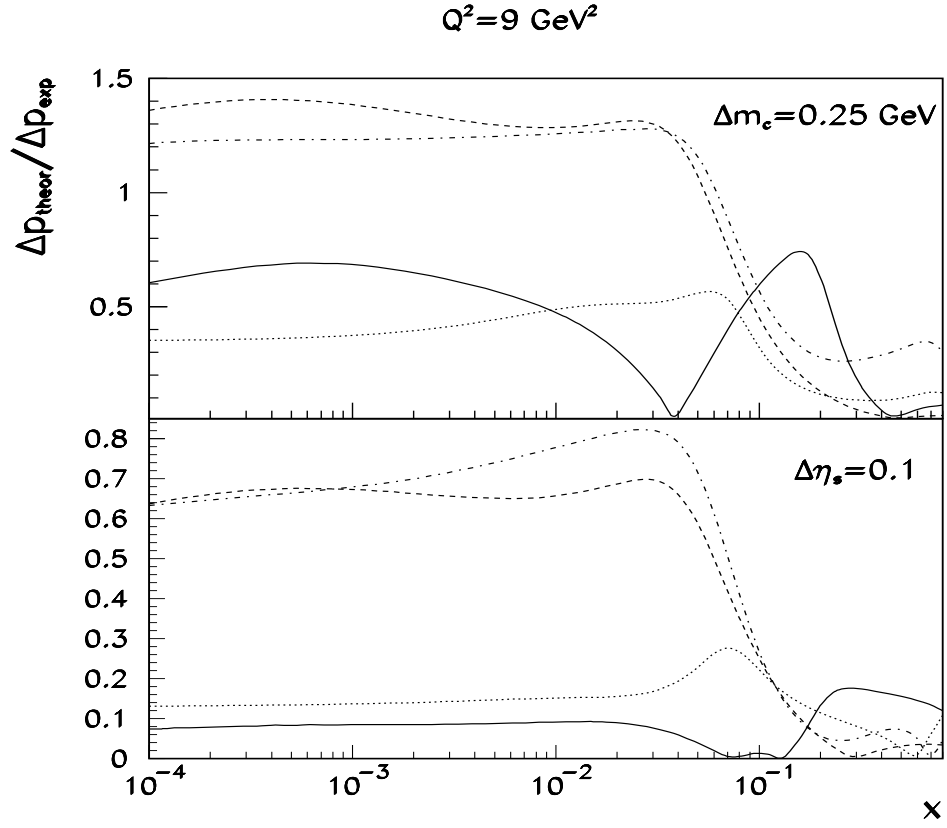


Figure 11: The ratio of magnitude of the uncertainty due to errors in the  $c$ -quark mass (upper panel) and the strange sea suppression factor (lower panel) to the experimental errors in NLO PDFs (full lines: gluon distribution; dashes: non-strange sea one; dots: d-quark one; dashed-dots: u-quark one).

uncertainty in value of  $\alpha_s$  as a separate theoretical error since we fit  $\alpha_s$  simultaneously with other parameters. In our previous analysis of Ref. [3] we considered the error due to uncertainty in the heavy-quarks thresholds in the QCD renormalization group equation for  $\alpha_s$ . Now we omit this error because it is generally negligible as compared to the experimental errors and other theoretical errors. The errors due to uncertainty in the nuclear effects in deuterium, which also was considered in Ref. [3], will be analyzed in details elsewhere [23].

## 5 High-twist contribution and the value of $\alpha_s$

In the analysis of DIS data with relatively low  $Q$  one needs to account for the HT terms due to these terms are essential part of the operator product expansion [24]. The HT terms cannot be accurately calculated from the existing theory of strong interaction and we have to account for them in our analysis phenomenologically. From comparison with the data we observe non-negligible contribution from the HT terms since account of such terms improves quality of the fit (e.g. in the NNLO fit the value of  $\chi^2$  rises by 330, if we fix the HT terms at 0). At the same time the observed HT terms can come just from the possible defects of the fitted model, in particular due to inaccount of the HO QCD corrections. Indeed, with the inclusion of the NLO correction in the analysis of data on the  $\nu N$  DIS the observed HT terms decrease and eventually vanish in the NNLO [25]. We also observe decrease of the HT terms with the pQCD order, but they do not vanish completely in our case (see Fig.12 and Table5). Extrapolation of the LO-NLO-NNLO results for the HT terms allows to expect that they should not vanish in the NNNLO also. This is in line with the conclusion of Ref. [26] that the HO corrections can successfully simulate power behavior in narrow region of  $x$  close to 0.1 only. This is also in agreement with the results of Ref. [27] (the effects of soft gluon resummation considered in Ref. [27] are important at  $x \gtrsim 0.8$  only and cannot further decrease the value of HT terms in our case). We see no contradiction between our results and the results of Ref. [25] in view of large errors in the HT terms extracted from the neutrino data, but do not support the conclusion about vanishing of the HT terms in the NNLO. The obtained HT contribution to  $F_2$  is maximal at  $x \sim 0.6$  and at  $Q^2 = 5 \text{ GeV}^2$  is  $\sim 10\%$  of the LT term. This is much larger than the value of the relative experimental error in the  $F_2$  measured in this region and

Table 4: Fitted coefficients of the HT contributions to the structure functions  $F_{2,L}$  in the NNLO

$x$	$H_2^P(x)$	$H_L^N(x)$
0.	$-0.034 \pm 0.022$	$0.234 \pm 0.037$
0.1	$-0.056 \pm 0.017$	$0.042 \pm 0.021$
0.2	$-0.019 \pm 0.011$	$0.055 \pm 0.021$
0.3	$-0.003 \pm 0.010$	$0.072 \pm 0.018$
0.4	$0.0077 \pm 0.0098$	$0.002 \pm 0.017$
0.5	$0.0299 \pm 0.0082$	$0.0138 \pm 0.0087$
0.6	$0.0469 \pm 0.0077$	$0.0060 \pm 0.0091$
0.7	$0.0447 \pm 0.0062$	$0.0233 \pm 0.0063$
0.8	$0.0398 \pm 0.0065$	$0.026 \pm 0.012$

Table 5: Values of  $\alpha_s(M_Z)$  obtained in different orders of pQCD.

LO	$0.1301 \pm 0.0026(\text{exp})$
NLO	$0.1171 \pm 0.0015(\text{exp})$
NNLO	$0.1143 \pm 0.0014(\text{exp})$

hence the account of the HT terms is indeed important.

Values of  $\alpha_s(M_Z)$  obtained in different orders of pQCD are given in Table 5. For comparison in the NNLO analysis of the existing data for DIS of charged leptons off proton the value of  $\alpha_s(M_Z) = 0.1166 \pm 0.0009$  (exp) was obtained [28]. This value is comparable with our result, but one is to note that, despite the low  $Q$  data were used in the fit, the analysis of Ref. [28] was performed with the HT terms fixed at zero. Meanwhile the values of  $\alpha_s$  and  $H_2$  at large  $x$  are strongly anti-correlated. From the trial fit with the constraint  $H_{2,L} = 0$  we obtain the value of  $\alpha_s(M_Z) = 0.1215 \pm 0.0003$  (exp), i.e. their value is much larger and their error is much smaller than in the fit with the HT terms fitted. From this comparison we conclude that in fact our result for  $\alpha_s$  is in disagreement with the result of Ref. [28]. In addition, value of  $\alpha_s$  obtained in the analysis of Ref. [28] rises from the NLO to the NNLO, in contrast with our results.



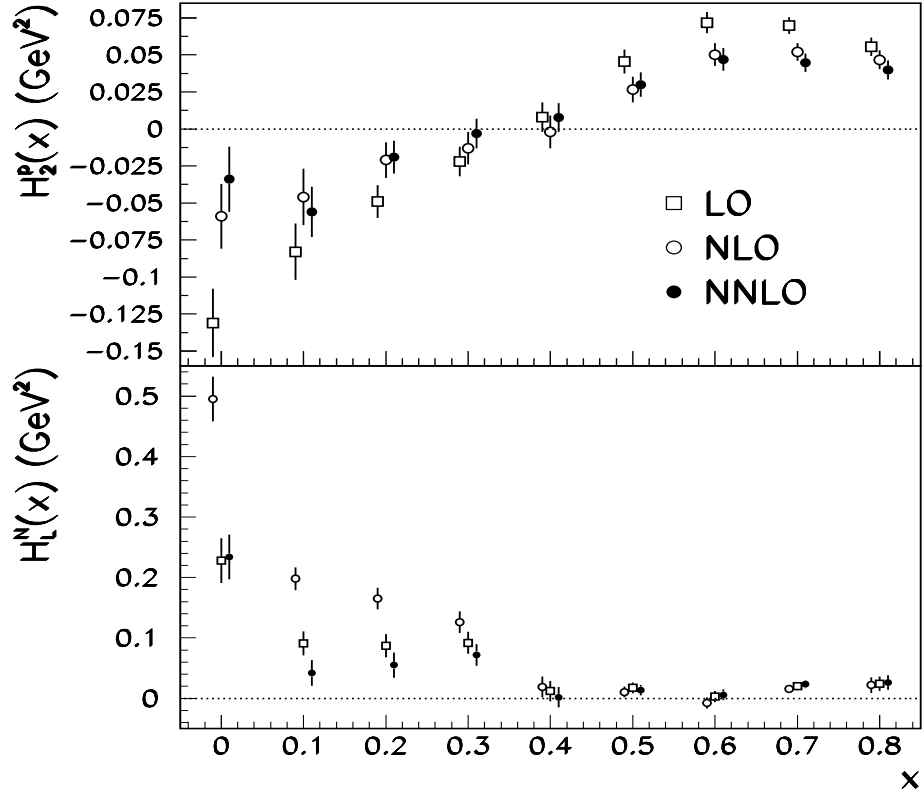


Figure 12: The HT contributions to the proton structure functions  $F_2$  (upper panel) and the nucleon structure function  $F_L$  (lower panel) obtained in the different orders of pQCD. For better view points are shifted to left and right along the  $x$ -axis.

## 6 Comparison with other parameterizations

Our NLO PDFs evolved in the VFN scheme are compared to the recent CTEQ and MRST parameterizations in Fig. 13. The comparison is made at  $Q^2 = 100 \text{ GeV}^2$ , which is the lowest scale for the hard processes at the hadron colliders. At this scale we observe the largest deviations of our PDFs from the CTEQ gluon distribution at large  $x$ , the MRST gluon distribution at small  $x$ , and the quark distribution of both groups at small  $x$ . The observed differences in particular can be due to the data on Drell-Yan process and jet production were used in the CTEQ and MRST analysis. To clarify this point thorough analysis of universality of the PDFs in different processes is necessary, but any way these differences can have impact on the calculated cross sections of hard processes at the hadron collider, e.g. on the K-factor for the Higgs boson production. The discrepancy with the MRST gluon distribution, which is the lowest of the three considered PDFs sets, is especially important since at small  $x$  it gets negative at small  $Q$ . At larger  $Q$  the difference between the different PDFs sets is smaller due to focusing properties of the QCD evolution [29].

Recently the CTEQ collaboration estimated the errors in their PDFs and we can compare those estimates with the errors in our PDFs. The comparison cannot be completely sensible since due to technical difficulties CTEQ did not take into account the impact of the normalization errors in data. Indeed, the account of normalization errors essentially increase the point-to-point correlations for many subsets and leads to amplification of the numerical instability of the calculations. The value of  $\Delta R$ , which is indicator of these correlations (see Sec.3), rises essentially if normalization errors are included into the covariance matrix. In particular, for the BCDMS data  $\Delta R$  is 0.68/0.29 with/without normalization errors taken into account. Meanwhile account of the normalization errors leads to increase of the PDFs uncertainties up to factor of 5 (see Fig.3). In the analysis of CTEQ the value of  $\chi^2/NDP$  for some data subsets deviates off 1 much more than this is statistically allowed. These fluctuations may be caused by several reasons, including inaccuracies in the model of data, such as inaccount of the HT terms, the target mass corrections, the nuclear corrections, and the HO QCD corrections. To avoid this problem CTEQ scaled their PDFs errors by the “tolerance” factor, which was selected equal to 10 in order to provide comparability of all data subsets. Effectively, the application of such tolerance factor leads to the crude account of all sources of uncertainties, including theoretical ones, since the scaled er-

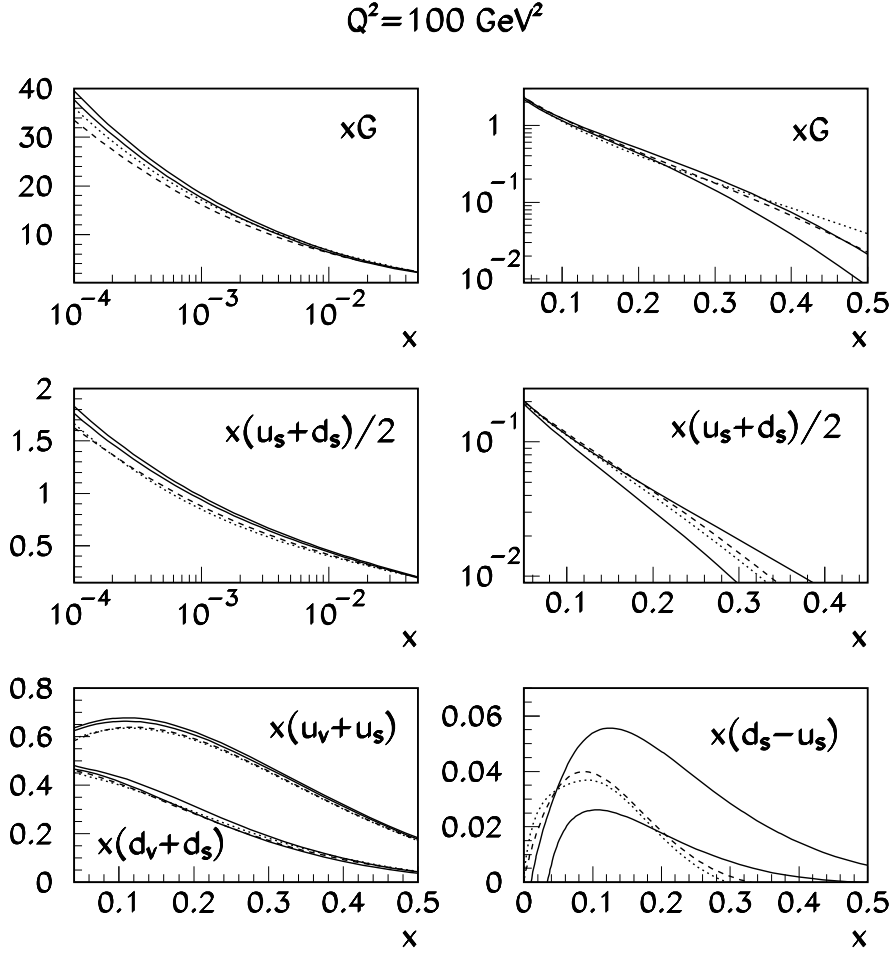


Figure 13: One-standard-deviation bands for our NLO PDFs evolved in the VFN scheme (full lines) compared to the MRST2001 (dashes) and CTEQ6 (dotes) PDFs.

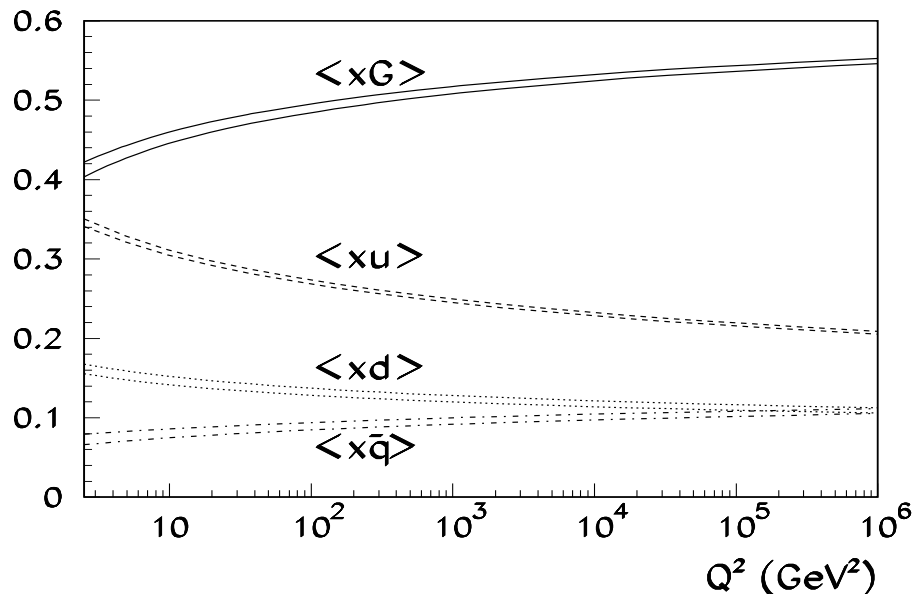


Figure 14: One-standard-deviation bands for the  $Q$ -dependence of the momentum carried by different parton species ( $\bar{q}$  reads sum of the anti-quark distributions).

errors cover the total range of possible variation of the fitted parameters. In our analysis we need not introduce the tolerance factor since deviations of  $\chi^2/NDP$  for separate data subsets off 1 fit to the possible statistical fluctuations (see Table 2). The errors in CTEQ6 PDFs are compared to ours in Fig. 2. For all PDFs, excluding the sea quarks distribution at  $x \sim 0.3$  the CTEQ PDFs errors are larger than ours. The difference is especially pronounced for the gluon and sea distributions at small  $x$  and for the  $u$ - and  $d$ -quark distributions at large  $x$ . From this comparison follows that use of the variety of data for the PDFs extraction not necessarily leads to the decrease of the PDFs errors since improvement in experimental accuracy can be accompanied by the growth of theoretical errors (at least one is to take care about accurate estimation of the later).

## 7 Access to the PDFs

The PDFs obtained in our analysis are available through the WWW page<sup>3</sup>. We placed in this page the PDFs generated in the LO, NLO, and NNLO; in the VFN and FFN schemes, including special sets with shifted values of the  $c$ -quark mass and the sea suppression factor to allow account of the corresponding theoretical uncertainties in PDFs. The PDFs are supplied by the experimental uncertainties, which can be conveniently taken into account in the calculation. This can be performed both using propagation error formula based on the PDFs derivatives and by generating random PDFs. The later way is most convenient in the Monte-Carlo calculations and was adopted in Les Houches interface for the PDFs with uncertainties [14]. The  $1\sigma$  bands for the first Mellin moments of the parton distributions at different  $Q^2$  calculated using this code are given in Fig.14. The typical uncertainties in the momentum carried by different species is generally less than 0.01, being the largest for the gluon distribution. The experimental errors in typical parton luminosities  $L$  for the antiproton-proton collisions at  $\sqrt{s} = 2$  TeV (Fermilab collider) and the proton-proton collisions at  $\sqrt{s} = 14$  TeV (LHC collider) are given in Fig.15. In the kinematical range relevant for the studies of hard processes the relative errors in parton luminosities for the LHC are in the range of  $1 \div 20\%$ ; for the Fermilab collider they are comparable with the LHC ones at  $M \lesssim 100$  GeV and are much larger at  $M \gtrsim 100$  GeV. The uncertainty in  $W$ -boson production cross section due to errors in PDFs is  $\sim 2\%$  for the both colliders; for the Higgs boson production cross section it is  $\sim 2\%$  for the LHC and varies from 2% to 10% for the Fermilab collider under variation of the Higgs boson mass from 100 GeV to 300 GeV.

## 8 Conclusion

The PDFs extracted from the DIS data only are precise enough: The estimated uncertainties in the parton luminosities including all sources of experimental errors in data are  $\lesssim 20\%$  in the kinematical region feasible at the LHC collider and  $\lesssim 60\%$  at the Fermilab collider. The theoretical errors in PDFs are under control and generally do not exceed experimental ones, therefore the DIS PDFs can be used for conclusive searches of deviation from

---

<sup>3</sup><http://sirius.ihep.su/~alekhin/pdfa02/>

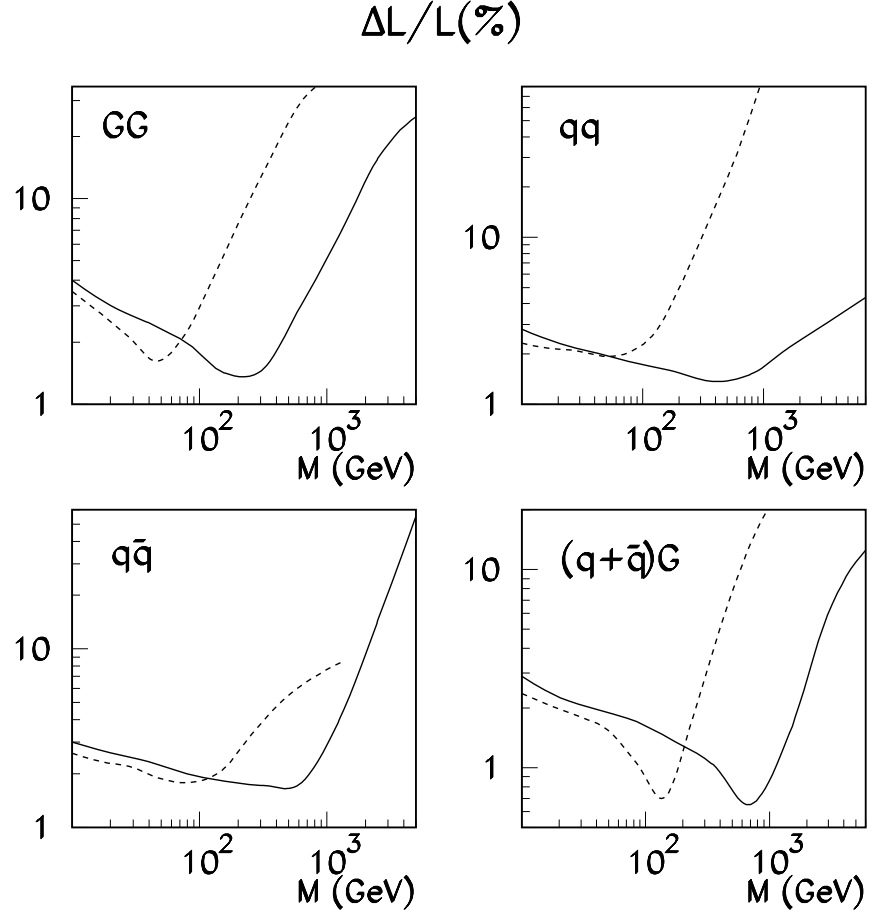


Figure 15: The dependence of parton-parton luminosities for the LHC (full curves) and the Fermilab collider (dashes) on the produced mass  $M$  ( $qq : L_{uu} + L_{dd} + L_{du}$ ;  $q\bar{q} : L_{u\bar{d}} + L_{d\bar{u}}$ ;  $(q + \bar{q})G : L_{uG} + L_{\bar{u}G} + L_{dG} + L_{\bar{d}G}$ ).

the Standard Model in other processes and/or checks of the universality of PDFs.

### Acknowledgments

I am indebted to E. Boos, M. Botje, W. Giele, A. Kataev, T. Sjostrand, W.K. Tung, and A. Vogt for stimulating discussions. The work was supported by the RFBR grant 00-02-17432.

## References

- [1] V. Barone, C. Pascaud and F. Zomer, Eur. Phys. J. C **12**, 243 (2000) [arXiv:hep-ph/9907512].
- [2] M. Botje, Eur. Phys. J. C **14**, 285 (2000) [arXiv:hep-ph/9912439].
- [3] S. Alekhin, Eur. Phys. J. C **10** (1999) 395 [arXiv:hep-ph/9611213];  
S. I. Alekhin, Phys. Rev. D **63** (2001) 094022 [hep-ph/0011002].
- [4] S. Aid *et al.* [H1 Collaboration], Nucl. Phys. **B470**, 3 (1996) [hep-ex/9603004].
- [5] M. Derrick *et al.* [ZEUS Collaboration], Z. Phys. **C72**, 399 (1996) [hep-ex/9607002].
- [6] C. Adloff *et al.* [H1 Collaboration], Eur. Phys. J. C **21**, 33 (2001) [arXiv:hep-ex/0012053].
- [7] S. Chekanov *et al.* [ZEUS Collaboration], Eur. Phys. J. C **21**, 443 (2001) [arXiv:hep-ex/0105090].
- [8] A. Retey and J. A. Vermaseren, Nucl. Phys. B **604**, 281 (2001) [arXiv:hep-ph/0007294].
- [9] W. L. van Neerven and A. Vogt, Phys. Lett. B **490**, 111 (2000) [arXiv:hep-ph/0007362].
- [10] S. I. Alekhin, Phys. Lett. B **519**, 57 (2001) [arXiv:hep-ph/0107197].
- [11] J. Pumplin, D. R. Stump, J. Huston, H. L. Lai, P. Nadolsky and W. K. Tung, [arXiv:hep-ph/0201195].

- [12] A. D. Martin, R. G. Roberts, W. J. Stirling and R. S. Thorne, [arXiv:hep-ph/0110215].
- [13] T. Adams *et al.* [NuTeV Collaboration], arXiv:hep-ex/9906037.
- [14] W. Giele *et al.*, arXiv:hep-ph/0204316.
- [15] S. I. Alekhin, arXiv:hep-ex/0005042.
- [16] C. Adloff *et al.* [H1 Collaboration], Eur. Phys. J. C **13**, 609 (2000) [arXiv:hep-ex/9908059].
- [17] M. R. Adams *et al.* [E665 Collaboration], Phys. Rev. D **54**, 3006 (1996).
- [18] E. Witten, Nucl. Phys. B **104** (1976) 445.
- [19] E. Laenen, S. Riemersma, J. Smith and W. L. van Neerven, Nucl. Phys. B **392** (1993) 229.
- [20] M. A. Shifman, A. I. Vainshtein and V. I. Zakharov, Nucl. Phys. B **136** (1978) 157 [Yad. Fiz. **27** (1978) 455].
- [21] J. C. Collins and W. K. Tung, Nucl. Phys. B **278** (1986) 934.
- [22] M. Gluck, E. Reya and M. Stratmann, Nucl. Phys. B **422** (1994) 37.
- [23] S. Alekhin, S. Kulagin, S. Luiti, in preparation.
- [24] K. G. Wilson, Phys. Rev. **179** (1969) 1499.
- [25] A. L. Kataev, G. Parente and A. V. Sidorov, Nucl. Phys. B **573** (2000) 405 [arXiv:hep-ph/9905310].
- [26] S. I. Alekhin, Phys. Lett. B **488** (2000) 187 [arXiv:hep-ph/9912484].
- [27] S. Schaefer, A. Schafer and M. Stratmann, Phys. Lett. B **514**, 284 (2001) [arXiv:hep-ph/0105174].
- [28] J. Santiago and F. J. Yndurain, Nucl. Phys. B **611** (2001) 447 [arXiv:hep-ph/0102247].
- [29] A. De Rujula, S. L. Glashow, H. D. Politzer, S. B. Treiman, F. Wilczek and A. Zee, Phys. Rev. D **10** (1974) 1649.